

Conductivity of twin-domain-wall/surface junctions in ferroelastics: Interplay of deformation potential, octahedral rotations, improper ferroelectricity, and flexoelectric coupling

Eugene A. Eliseev,¹ Anna N. Morozovska,^{2,*} Yijia Gu,³ Albina Y. Borisevich,⁴ Long-Qing Chen,³ Venkatraman Gopalan,³ and Sergei V. Kalinin⁴

¹*Institute for Problems of Materials Science, National Academy of Science of Ukraine, 3, Krjijanovskogo, 03142 Kiev, Ukraine*

²*Institute of Physics, National Academy of Science of Ukraine, 46, pr. Nauki, 03028 Kiev, Ukraine*

³*Department of Materials Science and Engineering, Pennsylvania State University, University Park, Pennsylvania 16802, USA*

⁴*Center for Nanophase Materials Science, Oak Ridge National Laboratory, Oak Ridge, Tennessee, 37831, USA*

(Received 20 May 2012; published 8 August 2012)

Electronic and structural phenomena at the twin-domain-wall/surface junctions in the ferroelastic materials are analyzed. Carriers accumulation caused by the strain-induced band structure changes originated via the deformation potential mechanism, structural order parameter gradient, rotostriction, and flexoelectric coupling is explored. Approximate analytical results show that inhomogeneous elastic strains, which exist in the vicinity of the twin-domain-wall/surface junctions due to the rotostriction coupling, decrease the local band gap via the deformation potential and flexoelectric coupling mechanisms. This is the *direct mechanism* of the twin-wall static conductivity in ferroelastics and, by extension, in multiferroics and ferroelectrics. On the other hand, flexoelectric and rotostriction coupling leads to the appearance of the improper polarization and electric fields proportional to the structural order parameter gradient in the vicinity of the twin-domain-wall/surface junctions. The “flexoroto” fields leading to the carrier accumulation are considered as an *indirect mechanism* of the twin-wall conductivity. Comparison of the direct and indirect mechanisms illustrates a complex range of phenomena directly responsible for domain-wall static conductivity in materials with multiple order parameters.

DOI: [10.1103/PhysRevB.86.085416](https://doi.org/10.1103/PhysRevB.86.085416)

PACS number(s): 77.65.-j, 73.25.+i, 62.20.D-

I. INTRODUCTION

The interactions between the soft-phonon driven lattice instabilities and electronic phenomena have fascinated physicists for more than half a century. Traditionally, the relevant areas included domain instabilities and light-induced phenomena in ferroelectrics,¹⁻⁵ electronic phenomena at the domain walls and surfaces.^{6,7} The first set of phenomena specifically addresses the interaction of ferroelectric order parameter fields with nonequilibrium charge carriers and has also found renewed interest due to ferroelectric photovoltaics.^{8,9} The second includes electronic^{2,10-12} and now electrochemical¹³⁻¹⁹ phenomena induced by ferroelectric polarization charge at surfaces and interfaces. From this perspective, ferroic walls offer arguably the simplest system for exploration of the interplay between ferroic and electronic phenomena due to continuity of atomic lattice and minimal contribution of chemical and electrochemical effects.

The earliest theoretical predictions of domain-wall conductivity in ferroelectric semiconductors was made by Guro *et al.*²⁰ in 1969, the mechanism originates from the compensation of polarization charge discontinuity by mobile carriers in the material. This model was further developed for uniaxial,^{21,22} multiaxial,²³ and improper ferroelectrics.²⁴ Numerous experimental justifications appeared after the development of scanning probe microscopy (SPM) techniques, capable of probing the conductance on the nanoscale, in multiferroic BiFeO₃,²⁵⁻²⁸ ferroelectrics Pb(Zr,Ti)O₃,^{29,30} ErMnO₃,³¹ and LiNbO₃ doped with MgO.³² Interestingly, the preponderance of the experimental results^{25-28,30} report about the conductivity of the nominally uncharged domain walls in multiferroics. Some of the recent studies demonstrate

hysteretic conductance of domain walls and presence of multiple remnant conduction states,^{26,30,33} a behavior ascribed to the role of metastable tilted wall configurations pinned by the structural defects. The recent report³⁰ on metallic conductivity of domain walls in Pb(Zr,Ti)O₃ provides strong evidence towards the semiconductor-ferroelectric model of charged domain walls.

However, the vast majority of materials that is now being explored in the context of domain wall mediated electronic phenomena possess multiple structural instabilities and are often incipient or proper ferroelectrics and ferroelastics. From this context, it is germane to consider the progression of theoretical models for wall structures. On the most basic level, works²¹⁻²³ consider the carrier accumulation by the strongly charged perpendicular (or “counter”) and inclined 180° ferroelectric domain using thermodynamical approach. Depending on the incline angle, the incline walls can be strongly charged, weakly charged, or uncharged.²³ Free carrier concentration, band bending, and enhanced electromechanical response at charged 90° domain walls in BaTiO₃ were recently considered in Ref. 34. Fiebig *et al.*³¹ demonstrated that the electrical conductance at the interfacial ferroelectric domain walls in hexagonal ErMnO₃ (and in analogous material YMnO₃) is a continuous function of the domain wall orientation, with a range of an order of magnitude variation between head-to-head and tail-to-tail domains walls. The variation is the combined consequence of carrier accumulation and band-structure changes at the walls. So, the origin of the charged domain-wall conductivity seems clear enough: the bound charge variation across the wall causes the electric field that in turn attracts screening carriers and causes band-structure changes.

However, the structural and electronic phenomena at the nominally uncharged domain walls in ferroelectrics-ferroelastics structures cannot be covered by the aforementioned studies.^{20–23,31,34} Recently, it was proposed^{23,30} that the flexoelectric coupling can lead to the appearance of inhomogeneous electric fields proportional to the polarization gradient across the nominally uncharged domain wall (called flexoelectric field^{23,30}) and to a field proportional to the structural order parameter gradient (called rotoflexo field^{35,36}). Notably, strain gradients are expected to induce polarization near the surfaces and interfaces via the flexoelectric effect^{37,38} in all materials, since they are flexoelectrics.^{39–41} Rotoflexo fields can then exist in a wide class of materials with oxygen octahedra rotations.⁴²

We further note that additional factors affecting the domain wall behavior are the strain and field-driven segregations of mobile ions. In particular, Salje *et al.*⁴³ have analyzed the surface structure of domain twin walls in ferroelastics using molecular dynamics simulations. Using analytical models, Rychetsky⁴⁴ considered the deformation of crystal surfaces in ferroelastic materials caused by antiphase domain boundaries. Using empirical force fields, Salje and Lee⁴⁵ numerically studied the interaction of oxygen vacancies in the ferroelastic CaTiO₃ [100] twin walls. Note, that improper ferroelectricity induced by octahedral rotations exists in YMnO₃,⁴⁶ Ca₃Mn₂O₇,⁴⁷ CaTiO₃,⁴⁸ and their interfaces.⁴⁹ In particular, Salje *et al.* directly observed ferroelectric polarization at ferroelastic domain boundaries in CaTiO₃ by aberration-corrected transmission electron microscopy (TEM) at room temperature.⁵⁰

We further note that exploration of domain-wall properties by scanning probe microscopy (SPM) necessarily involves probing not only the wall properties per se, but also the responses of the wall/surface junction since the latter is an inherent part of the conduction path. In comparison, a wall-back electrode junction is more distributed allowing for smaller resistances and higher contribution of defect-mediated conduction paths, and hence its properties are relatively less important. For the case of wall-surface junction, the relaxation of elastic stresses will lead to electric and/or elastic fields with power decay.^{51,52} Even for classical ferroelectrics, the carriers accumulation caused by the wall-surface junctions is studied only recently.⁵³ These considerations motivate us to study analytically free carriers accumulation caused by the twin-domain-wall/surface junctions in ferroelastics incipient ferroelectrics, and explore the role of improper ferroelectricity induced by the inhomogeneous octahedral rotations.

In this manuscript, we analytically solve the 2D problem of wall/surface junction for the model CaTiO₃ material. The paper is organized as following. Elastic fields caused by the twin-domain-wall/surface junction is calculated analytically and analyzed in Sec. II. In Sec. III, we consider the improper ferroelectricity appeared at the twin-domain-wall/surface junction. Section IV is devoted to the carrier accumulation at the twin-domain-wall/surface junction. Vacancy segregation at the twin-domain-wall/surface junction is estimated in Sec. V. The relevant mathematical details and materials parameters are provided in Supplemental Material.⁵⁴

II. ELASTIC FIELDS CAUSED BY THE TWIN-WALL/SURFACE JUNCTION

Here, we analyze the structure of the *elastic fields* created by the domain wall/surface junction in ferroelastics using the perturbation method proposed by Rychetsky.⁴⁴ In the first approximation, the surface displacement $u_i^S(\mathbf{x})$ at location \mathbf{x} induced by the elastic wall/surface junction is given by the convolution of the corresponding Green function with the elastic stress field, σ_{jk}^0 , unperturbed by the surface influence:

$$u_i^S(\mathbf{x}) = \int_{-\infty}^{\infty} d\xi_1 \int_{-\infty}^{\infty} d\xi_2 G_{ij}(x_1 - \xi_1, x_2 - \xi_2, x_3) \sigma_{jk}^0(\xi_1, \xi_2) n_k. \quad (1)$$

The corresponding Green's tensor $G_{ij}(\mathbf{x} - \xi)$ for an elastically isotropic half-space is given by Lur'e⁵⁵ and Landau and Lifshitz⁵⁶ (see Appendix A⁵⁴) and n_k is the outer normal to the mechanically free surface $x_3 = 0$. The geometry of calculations is shown in Fig. 1(a). Hereafter, we consider the semi-infinite mechanically free crystal, but not the film on the substrate. However, the approach can be extended to the film case if one will use the Green function corresponding to the elastic problem of mechanically clamped/free film.

Inhomogeneous elastic stresses $\sigma_{jk}^0(\xi_1, \xi_2)$ originate from the rotostriction coupling with the structural order parameter variation appeared in the vicinity of ferroelastic 90° twins. The order parameter describing oxygen octahedral rotations can be chosen either as the rotation angle or the displacement of an appropriate oxygen atom from its cubic position.^{57–59} The behavior of tetragonal ferroelastics (e.g., SrTiO₃ below 105 K) in the low-symmetry phase can be described by a single axial vector $\Phi = (\Phi_1, \Phi_2, \Phi_3)$,^{35,36,59} while description

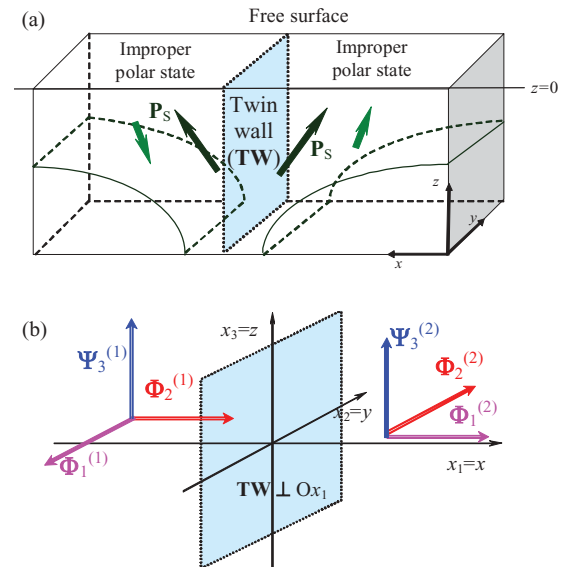


FIG. 1. (Color online) (a) Twin wall (TW) near the film surface. (b) Orientation of order parameters of the domains and TW with respect to pseudocubic axes Ox_1 , Ox_2 and Ox_3 for the case of head-to-tail TW. For orthorhombic ferroelastics, we consider 90° twins nonzero oxygen displacement nonzero components are Φ_1 , Φ_2 , and Ψ_3 . TW should be perpendicular to [100] or [010] directions. Coordinates $x_1 = x$, $x_2 = y$, and $x_3 = z$.

of orthorhombic ferroelastics (e.g., CaTiO₃ at room temperature) requires two axial vectors $\Phi = (\Phi_1, \Phi_2, \Phi_3)$ and $\Psi = (\Psi_1, \Psi_2, \Psi_3)$.⁶⁰

Here, for tetragonal ferroelastics, we consider 90° twins with nonzero oxygen displacement components Φ_1 and Φ_2 .⁵⁷ For orthorhombic ferroelastics, we consider that the 90° twins nonzero oxygen displacement nonzero components are Φ_1 , Φ_2 , and Ψ_3 [see Fig. 1(b)].⁶¹ In order to obtain approximate analytical expressions for σ_{jk}^0 unperturbed by the surface in orthorhombic ferroelastics, approximate analytical expressions for the structural order parameter components were used as $\Phi_1 \approx \Phi_S[1 + a \cosh^{-2}(x_1/w)]$, $\Phi_2 \approx \Phi_S \tanh(x_1/w)$, $\Psi_3 \approx \Psi_S[1 + b \cosh^{-2}(x_1/w)]$, where Φ_S and Ψ_S are spontaneous values, w is the intrinsic width of the twin wall in the bulk,

and the amplitudes a and b appeared much smaller than unity. Rigorously speaking, the wall width can be obtained from DFT calculations⁶² or STEM measurements,⁵⁰ and the profile functions are consistent with GLD theory and experiments. In Appendix B of Ref. 54, we list analytical expressions for several cases of the elastic stresses σ_{jk}^0 , namely, typical 90° twins in ferroelastics with tetragonal and orthorhombic space symmetries.

The strains $u_{kl}(x, z)$ can be calculated from Eq. (1) using the perturbation approach as $u_{kl}(x, z) = u_{kl}^0 + \frac{1}{2}(\frac{\partial u_{kl}^s}{\partial x_j} + \frac{\partial u_{kl}^s}{\partial x_i})$, where u_{kl}^0 is the strain field of the twin unperturbed by the surface. The stresses $\sigma_{kl}(x, z)$ are listed in Appendix B of Ref. 54. After lengthy calculations, we obtained Pade approximations⁶³ for nonzero strains:

$$u_{xx}(x, z) \approx u_{xx}^0 + \frac{(1+\nu)w\delta\sigma}{Y[x^2 + (w+z)^2]^3} \left(\frac{-(w^2+x^2)(w+z)^3 - x^2z[3w(w+z) + x^2]}{+[x^2 + (w+z)^2]\{z[x^2 + (w+z)^2] + 2w(w+z)^2\}v} \right), \quad (2a)$$

$$u_{xz}(x, z) \approx -\frac{(1+\nu)\delta\sigma wxz\{4w(w+z)^2 + z[x^2 + (w+z)^2]\}}{Y[x^2 + (w+z)^2]^3}, \quad u_{yy}(x, z) \approx u_{yy}^0, \quad (2b)$$

$$u_{zz}(x, z) \approx u_{zz}^0 + \frac{(1+\nu)w\delta\sigma}{Y[x^2 + (w+z)^2]^3} \left(\frac{-(w^2+3wz+z^2)(w+z)^3 - x^2(w^3+z^3)}{+[x^2 + (w+z)^2]\{z[x^2 + (w+z)^2] + 2w(w+z)^2\}v} \right). \quad (2c)$$

Here, ν is Poisson ratio, Y is the Young modulus, w is the intrinsic half-width of the twin wall in the bulk, coordinates $x_1 = x$, $x_2 = y$, and $x_3 = z$. The stress $\delta\sigma$ for the twins in tetragonal ferroelastics is listed in Appendix B.⁵⁴ The stress $\delta\sigma$ for the twins in orthorhombic ferroelastics:

$$\delta\sigma \approx \frac{s_{11}[R_{12} + (V_{122} + 6V_{112})\Phi_S^2] - s_{12}[R_{11} + (V_{111} + 6V_{112})\Phi_S^2]}{s_{11}^2 - s_{12}^2} \Phi_S^2. \quad (3a)$$

The strain field of the twin unperturbed by the surface is

$$u_{xx}^0 \approx R_{11}\Phi_S^2 + R_{12}\Phi_2^2 + V_{111}\Phi_S^4 + 6V_{112}\Phi_S^2\Phi_2^2 + V_{122}\Phi_2^4 + W_{122}\Psi_S^4 + \frac{s_{12}(\Phi_S^2 - \Phi_2^2)}{s_{11} + s_{12}} [R_{11} + R_{12} + (V_{111} + V_{122})(\Phi_S^2 + \Phi_2^2) + 6(V_{112} + V_{123})\Phi_S^2], \quad (3b)$$

$$u_{yy}^0 \approx (R_{11} + R_{12})\Phi_S^2 + (V_{122} + 6V_{112} + V_{111})\Phi_S^4 + W_{122}\Psi_S^4, \quad (3c)$$

$$u_{zz}^0 \approx 2R_{12}\Phi_S^2 + (2V_{122} + 6V_{123})\Phi_S^4 + W_{111}\Psi_S^4. \quad (3d)$$

Elastic compliances s_{ijkl} , the fourth-order rotostriction coefficients R_{ijkl} and the sixth-order rotostriction coefficients V_{ijklmn} and W_{ijklmn} are written in Vought notations. Note that sixth-order rotostriction cannot be omitted if one aims at a correct description of CaTiO₃ structural and elastic properties, otherwise it is impossible to describe correctly the structural phase diagram of the bulk material (see Table C3 in the end of Appendix C of Ref. 54). Let us underline that the strains (2) are proportional to the product of corresponding rotostriction coefficients, the second and fourth powers of the oxygen displacement components. So, the strains appearance is the typical manifestation of the rotostriction effect.

Note that the u_{yy}^0 and u_{zz}^0 are spontaneous strains that exist in the bulk stress-free single-domain sample. The strain u_{xx}^0 contains the spontaneous part and the part proportional to the

order parameter variation ($\Phi_S^2 - \Phi_2^2$), which vanishes far from the twin wall. The appearance of the nonzero out-of-plane strain $u_{zz}(x, 0)$ is related with the appearance of a topographic defect (“ditch”) on the surface, located at the wall region $x = 0$, rather than with the limited accuracy of the approximation. Elastic stresses given by Eq. (3) decay by a power law away from wall-surface junction both in x and z directions.

Finally, to describe the carrier accumulation at the wall-surface junction, we are also interested in the trace of the strain tensor that can be found as

$$Tr(u_{ij}) \equiv u_{ii} \approx u_{xx}^0 + u_{yy}^0 + u_{zz}^0 - \frac{\delta\sigma(1+\nu)(1-2\nu)}{Y} \times \frac{w\{2w(w+z)^2 + z[x^2 + (w+z)^2]\}}{[x^2 + (w+z)^2]^2}. \quad (4)$$

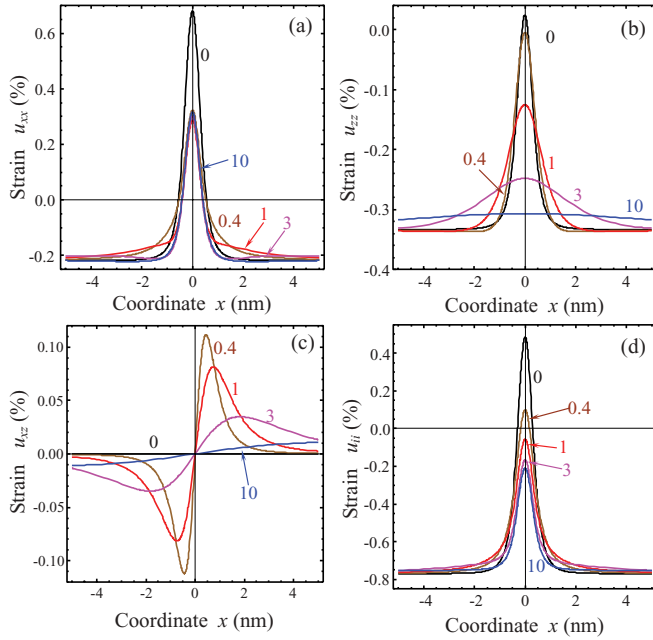


FIG. 2. (Color online) Strain components $u_{xx}(x,z)$ (a), $u_{zz}(x,z)$ (b), $u_{xz}(x,z)$ (c) and trace of the strain tensor $u_{ii}(x,z)$ (d) vs the distance x from the twin-wall plane $x = 0$ calculated at different distances z from the surface (numbers near the curves) for CaTiO_3 parameters and room temperature (see Table C3 in Ref. 54). Half-width of the twin wall in the bulk is taken as $w = 0.5$ nm.

Note, that Eqs. (2)–(4) provide the first-order approximations for strains that do not include polarization-dependent components, e.g., induced electrostriction and flexoelectric coupling. Numerical solution of the nonlinear coupled problem (see Appendix C in Ref. 54 for details) proved that improper polarization induced by the flexoroto effect^{35,36} in ferroelastic CaTiO_3 is relatively small (see Sec. II B) and thus the first approximation becomes grounded and consistent. In particular, if we account for the flexoelectric effect contribution in Eq. (3), it leads to the small second-order correction in polarization proportional to the square of the flexoelectric coupling coefficient.

The strain $u_{xx}(x,z)$, $u_{zz}(x,z)$, $u_{xz}(x,z)$ fields and trace of the strain tensor $\sum_{i=1}^3 u_{ii}(x,z)$ fields in the vicinity of wall-surface junction for CaTiO_3 at room temperature are shown in Fig. 2. Note that the strain $u_{zz}(x,z)$ and the trace $\text{Tr}(u_{ij}) \equiv \sum_{i=1}^3 u_{ii}(x,z)$ have a pronounced maximum ($\sim 0.5\%$) at $x = 0$. The strain amplitude decreases and the half-width increases away from the surface. The strain profile $u_{xx}(x,z)$ splits in two maxima. As expected, deep in the material the strains tend to the spontaneous values u_{xx}^0 and u_{zz}^0 . The strains $u_{xx}(x,z)$ and $u_{zz}(x,z)$ are symmetric with respect to the wall plane $x = 0$. The shear strain $u_{xz}(x,z)$ is symmetric with respect to the wall plane $x = 0$; it has two maxima whose amplitude strongly decreases when z increases. Interestingly, the scale of the strains amplitude decay is about 10 nm, i.e., well within the applicability limit of mesoscopic theory. The scale is an order of magnitude higher than the domain wall width $w = 0.5$ nm, since the strains decrease follows the long-range power law in accordance with Eqs. (2)–(4). Below, we will show that the

long-range decay could strongly affect the appearance of the improper polarization and especially on carriers accumulation caused by the wall-surface junction.

III. IMPROPER FERROELECTRICITY AT THE TWIN-DOMAIN-WALL/SURFACE JUNCTION

Here, we explore spontaneous polarization induced by flexoelectric coupling in the vicinity of the twin-domain-wall/surface junction, as derived in Appendix C of Ref. 54. Since the values of the gradient coefficients and their anisotropy are yet unknown for CaTiO_3 , here we did not list the results of numerical simulations based on the free energy minimization. The approximate analytics used hereinafter does not require the knowledge of the coefficients; only the width of domain wall w is included. However, this is a questionable benefit of the analytical treatment, since the anisotropy of the coefficients essentially influences the structural order parameter behavior in, e.g., SrTiO_3 .^{57,59} Flexoelectric coefficients are also unknown for CaTiO_3 , but the knowledge of their exact values is not very critical for calculations, since the symmetry and their order of magnitude are well-known and relatively high for perovskites.

Polarization fields originating from flexoelectric coupling can be estimated as

$$P_i(x,z) \approx \alpha_{ij}^{-1} \left(f_{mnlj} \frac{\partial u_{mn}}{\partial x_l} - \frac{\partial \varphi}{\partial x_j} \right). \quad (5)$$

Flexoelectric tensor coefficients are denoted as f_{mnlj} , whose numerical values, $f_{11} = -3.24$ V, $f_{12} = 1.44$ V, and $f_{44} = 1.08$ V, were determined experimentally for SrTiO_3 ,⁶⁴ for BaTiO_3 , $f_{12} = 450$ V was determined experimentally^{65,66} and $f_{11} = 5.12$ V, $f_{12} = 3.32$ V, and $f_{44} = 0.045$ V were calculated theoretically.⁶⁷ Estimations from Kogan model give $f_{ij} \sim 3.6$ V.⁶⁸

The electrostatic potential φ can be determined from the Poisson equation, $\epsilon_0 \epsilon_b \frac{\partial^2 \varphi}{\partial x_i^2} = \frac{\partial P_i}{\partial x_i} - e(p - n + N_d^+ - N_a^-)$, where $\epsilon_0 = 8.85 \times 10^{-12}$ F/m is the universal dielectric constant, ϵ_b is the background dielectric permittivity unrelated to the soft mode permittivity $\epsilon_{ij}^{sm} = \epsilon_0^{-1} \alpha_{ij}^{-1}$, and $e = 1.6 \times 10^{-19}$ C is the absolute value of the electron charge; $p(\varphi)$ and $n(\varphi)$ are the electron and hole densities, respectively; N_d^+ and N_a^- are the concentration of ionized acceptors and donors, respectively. The situation when depolarization effects can be negligibly small in comparison with the flexoelectric polarization $\delta P_i^{flexo}(x,z) \sim \alpha_{ij}^{-1} f_{mnlj} \frac{\partial u_{mn}}{\partial x_l} \sim \epsilon_0 \epsilon_{ij}^{sm} f_{mnlj} \frac{\partial u_{mn}}{\partial x_l}$ corresponds to short-circuit electrical boundary conditions. For open-circuit boundary conditions, $P_i(x,z) \sim \frac{\epsilon_b}{\epsilon_b + \epsilon_{ij}^{sm}} f_{mnlj} \frac{\partial u_{mn}}{\partial x_l}$, and so it can be much smaller if $\epsilon_b \ll \epsilon_{ij}^{sm}$. The usage of short-circuit electrical boundary conditions is justified if the surface is covered by the perfectly conductive layer (metallic electrode). An electroded surface is one of typical experimental conditions.

Coefficients $\alpha_{ij}(T,x,z)$ are affected by elastic fields and biquadratic coupling as³⁶

$$\alpha_{ij}(T,x,z) = a_{ij}(T) - q_{ijkl} u_{kl}(x,z) - \eta_{ijkl} \Phi_k \Phi_l - \xi_{ijkl} \Psi_k \Psi_l. \quad (6)$$

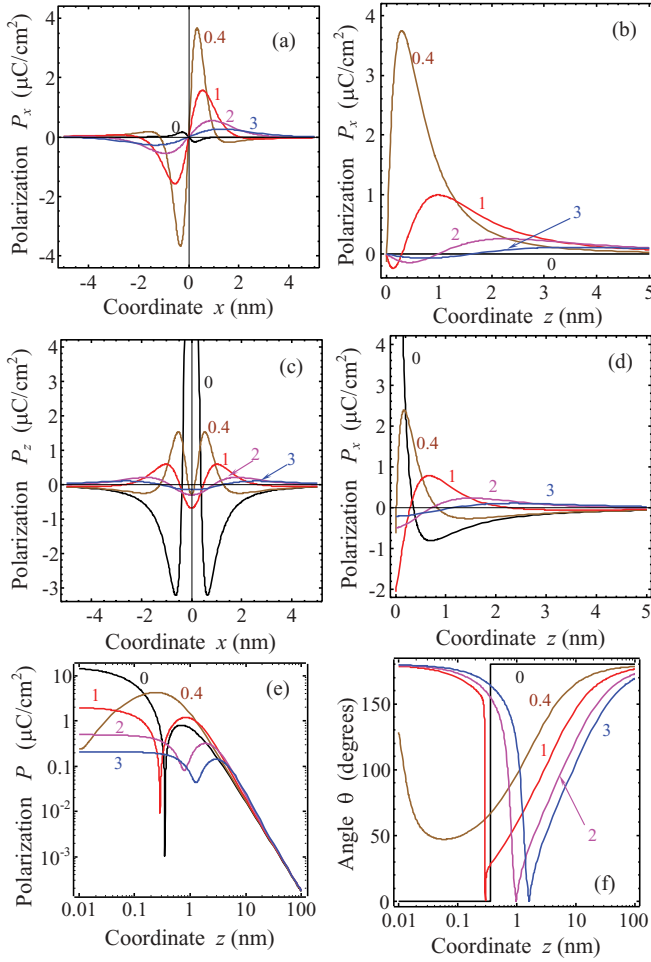


FIG. 3. (Color online) In-plane $P_x(x,z)$ (a) and out-of-plane $P_z(x,z)$ (c) polarization components vs the distance x from the twin-wall plane $x = 0$ calculated at different distances z from the CaTiO_3 surface (numbers near the curves). In-plane $P_x(x,z)$ (b) and out-of-plane $P_z(x,z)$ (d) polarization vs the distances z from the CaTiO_3 surface calculated at different distances x from the twin-wall plane $x = 0$ (numbers near the curves). Log-log plots of polarization amplitude $P = \sqrt{P_x^2 + P_z^2}$ (e) and tilting angle $\theta = \arccos(P_z/P)$ (f). Flexoelectric coefficients $f_{11} = 16$ V, $f_{12} = -7$ eV, and $f_{44} = 5$ V. Other parameters are the same as in Fig. 2.

The temperature dependence of the coefficient $a_{ii}(T)$ can be described by the Barrett law for SrTiO_3 ⁶⁹ and CaTiO_3 ,⁶⁰ q_{ijkl} are electrostriction coefficients, η_{ijkl} and ξ_{ijkl} are the biquadratic coupling tensor coefficients between the structural and polar order parameters.^{70,71} The elastic stresses induced by the twin-domain-wall/surface junction appeared too small to induce ferroelectric polarization in CaTiO_3 at room temperature, i.e., $\alpha_{ij}(T, x, z)$ is always positive.

The polarization behavior is primary determined by the strain gradient convolution with the flexoelectric effect tensor in accordance with Eq. (5). Since the strains are proportional to the product of the corresponding rotostriction coefficients and the second (or forth) powers of the oxygen displacement components, it can be concluded that in this case the improper polarization (5) is caused by the flexoroto effect.^{35,36}

The spatial distributions of the in-plane $P_x(x,z)$ and out-of-plane $P_z(x,z)$ polarization components are shown in Figs. 3(a)

and 3(c). As expected, the $P_x(x,z)$ profiles are antisymmetric and the $P_z(x,z)$ profiles are symmetric with respect to the wall plane $x = 0$. The polarization profiles have two maxima in the vicinity of the wall plane, whose amplitude strongly decreases and the half-width increases with increasing z more than one lattice constant. The result seems to be in qualitative agreement with TEM results.⁵⁰

Dependencies of the in-plane $P_x(x,z)$ and out-of-plane $P_z(x,z)$ polarization components on the distance z from the CaTiO_3 surface are shown in Figs. 3(b) and 3(d) at different distances x from the twin-wall plane $x = 0$. The polarization component $P_x(x,z)$ has a pronounced maximum at the surface $z = 0$, then it strongly vanishes and diffuses with increasing z . z dependencies are nonmonotonic with a pronounced maximum whose amplitude decreases and the z location increases with increasing x . $P_x(0,z)$ is identically zero as anticipated from the symmetry consideration. $P_z(0,z)$ is maximal under the surface and its value is noticeable ($> 3 \mu\text{C}/\text{cm}^2$).

The characteristic depth scale of the polarization amplitude decay is about 2–3 nm. The polarization value becomes negligibly small at distances ~ 5 nm from the surface. Similarly to elastic strains, the polarization decay obeys the long-range power law in accordance with Eqs. (2)–(4) and (5). This behavior is illustrated in log-log plots in Figs. 3(e) and 3(f) for polarization amplitude $P = \sqrt{P_x^2 + P_z^2}$ and tilting angle $\theta = \arccos(P_z/P)$. The spontaneous polarization $P \sim 1 \mu\text{C}/\text{m}^2$ predicted for the depth of $z \sim 100$ nm is much higher than the polarization reported for multiferroics-improper ferroelectrics $\sim 1 \text{ nC}/\text{m}^2$.⁷² The power-law decay of the polarization induced by elastic field at the twin-domain-wall/surface junction is fundamentally different from the exponential decay of the polarization induced by the homogeneous de-twinning ferroelastic surface reported earlier.³⁶

IV. CARRIERS ACCUMULATION AT THE TWIN-DOMAIN-WALL/SURFACE JUNCTION

In this section, we explore the coupling between order parameter fields and the band structure. In deformation potential theory,^{73–78} the strain induced conduction (valence) band edge shift caused by the wall-surface junction is proportional to the strain variation $u_{ij}^S(x,z) = u_{ij}(x,z) - u_{ij}^0(|x| \rightarrow \infty)$ given by Eq. (2), where $u_{ij}^0(|x| \rightarrow \infty)$ is the corresponding spontaneous strain given by Eq. (2) in the limit $\Phi_2^2 \rightarrow \Phi_3^2$. Thus

$$\begin{aligned} E_C(u_{ij}^S(x,z)) &= E_{C0} + \Xi_{ij}^C u_{ij}^S(x,z), \quad E_V(u_{ij}^S(x,z)) \\ &= E_{V0} + \Xi_{ij}^V u_{ij}^S(x,z), \end{aligned} \quad (7)$$

where E_C and E_V are the energetic positions of the bottom of conduction band and the top of the valence band, respectively,⁷⁹ $\Xi_{ij}^{C,V}$ is a tensor deformation potential of electrons in the conduction (C) and valence bands (V), where values $E_{C0} = E_C(u_{ij}^0(|x| \rightarrow \infty))$ and $E_{V0} = E_V(u_{ij}^0(|x| \rightarrow \infty))$. The symmetry of the deformation potential tensors $\Xi_{ij}^{C,V}$ is rather complex, but it coincides with the crystal spatial symmetry at the Γ point.⁷⁶ Below, we use the cubic parent phase approximation of the deformation potential for numerical calculations, i.e., $\Xi_{ij}^{C,V} = -\Xi_d^{C,V} \delta_{ij}$ (δ_{ij} is a

Kronecker δ symbol), since the spontaneous tetragonal or orthorhombic distortions are absent in the parent phase. Typical absolute values of $\Xi_d^{C,V}$ are ~ 8 – 12 eV for Ge (see Table II in Ref. 74), 21 eV extracted from experimental data for BiFeO₃,⁸⁰ 8 eV for SrTiO₃ estimated from *ab initio* calculations,⁸¹ but still poorly studied for both ferroelectrics and ferroelastics. Below we use the value 8 eV⁸¹ for numerical estimations in CaTiO₃. Note that both for tetragonal SrTiO₃ and orthorhombic CaTiO₃ nondiagonal components of deformation potential should be absent.

The electric field $E_i = -\partial\varphi/\partial x_i$ and electrostatic potential φ are determined self-consistently from the Poisson equation, where the polarization $\delta P_i^{\text{flexo}}(x,z) \sim \alpha_{ij}^{-1} f_{mnl} \frac{\partial u_{mn}}{\partial x_l}$ can be taken as zero order within adopted perturbation approach. The variation of the electric field related with the flexoelectric effect is $\delta E_j^{\text{flexo}} \sim -\frac{f_{mnl}}{1+\epsilon_0\epsilon_f\alpha_{11}} \frac{\partial u_{mn}}{\partial x_l} \sim -f_{mnl} \frac{\partial u_{mn}}{\partial x_l}$. Since u_{mn} is proportional to the product of corresponding rotostriction coefficients and the second (or forth) powers of the oxygen displacement components, the field $\delta E_j^{\text{flexo}}$ is in fact the so-called flexoroto field.^{35,36} The corresponding electric potential variation $\delta\phi_{\text{flexo}}$ caused by the field $\delta E_j^{\text{flexo}}$ is $\delta\phi_{\text{flexo}}(x,z) = -\int_{-\infty}^z dz' \delta E_z(x,z') = f_{mn33} u_{mn}^S(x,z)$.

Allowing for the deformation and electric potential variation and flexoelectric mechanism, local band bending caused by the twin-domain-wall/surface junction can be estimated as $\Delta E_n(x,z) = \Xi_d^C u_{ii}^S(x,z) + e\delta\phi_{\text{flexo}}(x,z)$ for electrons and $\Delta E_p(x,z) = -\Xi_d^V u_{ii}^S(x,z) - e\delta\phi_{\text{flexo}}(x,z)$ for holes. The band bending and changes in electrochemical potentials modulate the densities of free electrons $n(x,z)$ and holes $p(x,z)$ accumulated by the wall/surface junction. The effect can be estimated within the Boltzmann approximation as

$$n(x,z) \approx n_0 \exp \left[\frac{\Xi_d^C u_{ii}^S(x,z) + e f_{ij33} u_{ij}^S(x,z)}{k_B T} \right], \quad (8a)$$

$$p(x,z) \approx p_0 \exp \left[\frac{-\Xi_d^V u_{ii}^S(x,z) - e f_{ij33} u_{ij}^S(x,z)}{k_B T} \right]. \quad (8b)$$

Here, $k_B = 1.3807 \times 10^{-23}$ J/K and T is the absolute temperature.

Equation (8) describes the additive effect of deformation potential and flexoelectric coupling on the carrier density and local band bending [see also Eqs. (19) and (20) in Ref. 82]. We further note that these equations are valid only as the first-order approximation, since polarization and structural order parameters are coupled with each other as well as with elastic fields. Strains also contain a polarization-dependent part (via electrostriction effect) and flexoelectric contribution, but all the corrections appeared small and should be considered only in the second order of the perturbation theory.

The static conductivity $\rho(x,z)$ is proportional to the carriers densities (7) as $\rho(x,z) = e\mu_n n(x,z) + e\mu_p p(x,z)$, where e is the electron charge, mobilities $\mu_{n,p}$ are regarded constant. Within the model, the terms $\Xi_d^C u_{ii}^S(x,z)$ and $\Xi_d^V u_{ii}^S(x,z)$ in Eq. (7) related with deformation potentials explain the *direct mechanism* of the twin domain-wall static conductivity increase in the semiconducting and insulating ferroelastics and by extension in multiferroics. The trace of the strain tensor $u_{ii}(x,z)$ for considered problem is given by Eq. (4).

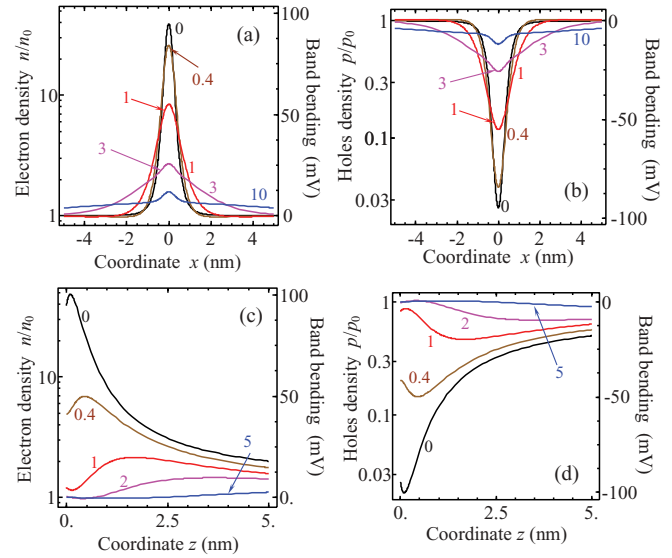


FIG. 4. (Color online) (a) and (b) Relative carriers density (left scale) and local band bending (right scale) vs the distance x from the twin-wall plane $x = 0$ calculated at different distances z from the CaTiO₃ surface (numbers near the curves). (c) and (d) Relative carriers density (left scale) and local band bending (right scale) vs the distances z from the CaTiO₃ surface calculated at different distances x from the twin wall plane $x = 0$ (numbers near the curves). Deformation potentials $\Xi_d^C = \Xi_d^V = 8$ eV, flexoelectric coefficients $f_{11} = 16$ V, $f_{12} = -7$ eV, and $f_{44} = 5$ V. Other parameters are the same as in Fig. 2.

As shown previously,^{35,36} the flexoelectric coupling leads to the appearance of inhomogeneous electric fields proportional to the polarization gradient across the wall (flexoelectric field) and to the structural order parameter gradient (rotoflexo field). The fields, which exist at the twin-wall/surface junctions, lead to the carrier accumulation via $\delta\phi_{\text{flexo}}(x,z) = f_{mn33} u_{mn}^S(x,z) \sim f_{ij33} R_{ijkl} \Phi_k \Phi_l$. Here, we refer to the changes of electrochemical potential due to flexoelectric effect, $\pm e f_{ij33} u_{ij}^S(x,z)$ in Eqs. (8), as the *indirect mechanism* of domain-wall conductivity.

The local band bending (in linear scale) and carrier density (in log-linear scale) are shown in Figs. 4(a) (electrons) and (b) (holes). The profiles are symmetric with respect to the wall plane $x = 0$ and have a sharp maximum at $x = 0$ and small z values. The maximal amplitude decreases and its half-width increases with increasing z . The depth profiles of the local band bending and carrier density are shown in Figs. 4(c) (electrons) and 4(d) (holes) at different distances x from the twin-wall plane $x = 0$. Z dependencies are nonmonotonic with a maximum, which amplitude decreases with x increase.

For the model case $\Xi_d^C = \Xi_d^V$, the deformation potential mechanism contributes equally to the electron and hole accumulation by the walls [see Eq. (8)], while the difference between electron and hole band bending originates from the flexoelectric coupling and is equal to $-2e f_{mn33} u_{mn}^S(x,z)$. In numbers, the difference of the accumulated carrier densities appears in the vicinity of the junction. The electrons density near the surface can be about 10–40 times higher than the bulk one, while the holes density near the surface can be much smaller than the bulk one for the realistic values of deformation

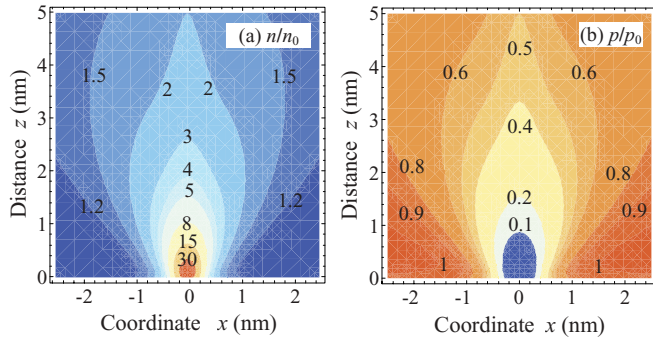


FIG. 5. (Color online) Contour maps of the electron (a) and hole (b) densities in the vicinity of the twin-wall/surface junction in CaTiO₃. The twin-wall plane is $x = 0$. Other parameters are the same as in Fig. 4.

potential $\Xi_d^{C,V} = 8$ eV and flexoelectric coefficients $f_{11} = 16$ V, $f_{12} = -7$ eV, and $f_{44} = 5$ V. Hence the flexoelectric coupling sign is primary responsible for the twin-wall n -type (or p -type) conductivity in ferroelastics proper semiconductors. Consequently, the strength of the indirect contribution can be estimated from the difference of the electron and hole densities accumulated by the twin walls. For the material parameters used, the relative contributions of deformation potential and flexoelectric coupling into the carrier accumulation are of the same order. For materials with weak flexoelectric coupling (such as SrTiO₃ with $f_{11} = 1.6$ V, $f_{12} = -0.7$ eV, and $f_{44} = 0.5$ V⁶⁴), the deformation potential contribution should dominate. It is seen from the contour maps of the electron [see Fig. 5(a)] and hole [see Fig. 5(b)] densities that the characteristic scale of the carrier density variation is about 5 nm.

V. VACANCY SEGREGATION AT THE TWIN-DOMAIN-WALL/SURFACE JUNCTION

Similarly to the electron accumulation and hole depletion, the twin-domain-wall/surface junction in CaTiO₃ (or SrTiO₃) can accumulate donors (oxygen vacancies) or acceptors (titanium vacancies). Here, the Vegard expansion (elastic dipole) tensor $\beta_{jk}^{a,d}$ plays the same role in the vacancy segregation as the deformation potential tensor in the electron accumulation. The structure of Vegard expansion tensor is controlled by the symmetry (crystalline or Curie group symmetry) of the material. For isotropic or cubic media, it is diagonal and reduces to scalar: $\beta_{ij}^{a,d} = \beta_{ii}^{a,d} \delta_{ij}$.⁸³

Using analytical expressions for single-ionized donors concentration $N_d^+ \approx N_{d0}^+ \exp[(\beta_{jk}^d u_{jk} - e\phi)/k_B T]$ and $N_a^- \approx N_{a0}^- \exp[(\beta_{jk}^a u_{jk} + e\phi)/k_B T]$ for single-ionized acceptors concentration (derived in Ref. 82) and the expression for the potential variation $\delta\phi_{flexo}(x,z) = f_{mn33} u_{mn}^S(x,z)$, the corresponding analytical expressions have the form:

$$N_d^+(x,z) \approx N_{d0}^+ \exp \left[\frac{\beta_{ii}^d u_{ii}^S(x,z) - e f_{ij33} u_{ij}^S(x,z)}{k_B T} \right], \quad (9a)$$

$$N_a^-(x,z) \approx N_{a0}^- \exp \left[\frac{\beta_{ii}^a u_{ii}^S(x,z) + e f_{ij33} u_{ij}^S(x,z)}{k_B T} \right]. \quad (9b)$$

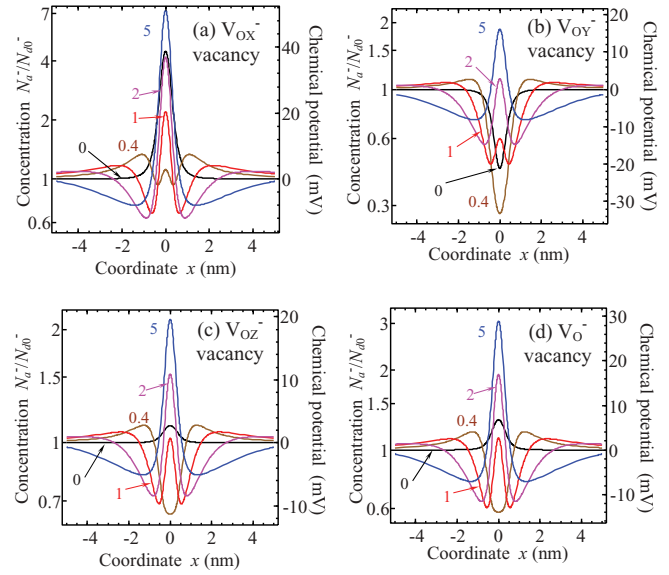


FIG. 6. (Color online) (a) and (b) Relative concentration of single-ionized O vacancies (left scale) and their electrochemical potential variation (right scale) vs the distance x from the twin-wall plane $x = 0$ calculated at different distances z from the CaTiO₃ surface (numbers near the curves). Elastic dipole tensor $\beta_{22}^d = \beta_{33}^d = -2.13$ eV, $\beta_{11}^d = 4.53$ eV for vacancy orientation V_{OX}^- (a); $\beta_{11}^d = \beta_{33}^d = -2.13$ eV, $\beta_{22}^d = 4.53$ eV for vacancy orientation V_{OY}^- (b); $\beta_{11}^d = \beta_{22}^d = -2.13$ eV, $\beta_{33}^d = 4.53$ eV for vacancy orientation V_{OZ}^- (c); $\beta_{ii}^d = 0.09$ eV for V_O^- vacancy (d). Other parameters are the same as in Fig. 4.

Here, N_{d0}^+ and N_{a0}^- are the concentration of single-ionized vacancies in the bulk. For neutral vacancies, the corresponding expressions are $N_d^0(x,z) \approx N_{d0} \exp[\frac{\beta_{ii}^d u_{ii}^S(x,z)}{k_B T}]$ and $N_a^0(x,z) \approx N_{a0} \exp[\frac{\beta_{ii}^a u_{ii}^S(x,z)}{k_B T}]$.

For numerical estimations of the O vacancies accumulation, we use the anisotropic values of the elastic dipole tensor $\beta_{22}^d = \beta_{33}^d = -2.13$ eV, $\beta_{11}^d = 4.53$ eV (vacancy orientation V_{OX}^-), $\beta_{11}^d = \beta_{33}^d = -2.13$ eV, $\beta_{22}^d = 4.53$ eV (vacancy orientation V_{OY}^-), $\beta_{11}^d = \beta_{22}^d = -2.13$ eV, $\beta_{33}^d = 4.53$ eV (vacancy orientation V_{OZ}^-) and the isotropic average $\beta_{ii}^d = 0.09$ eV (V_O^- vacancy) as calculated by Freedman *et al.*⁸³ For Ti vacancy, we use the values $\beta_{11}^a = \beta_{22}^a = \beta_{33}^a = 28$ eV.⁸³ Profiles of the electrochemical potential $\chi_d(x,z) = \beta_{ii}^d u_{ii}^S(x,z) - e f_{ij33} u_{ij}^S(x,z)$ and concentration of O vacancies (in log-linear scale) are shown in Fig. 6 at different distances z from the CaTiO₃ surface and room temperature. The vacancy concentration can be higher than the bulk one by 2–7 times (compare the result with Ref. 45). In the surface plane, the profiles are symmetric with respect to the wall plane $x = 0$ and have a sharp maximum (or minimum) at $x = 0$. The maximum (minimum) amplitude decreases and its half-width increases with increasing z . For $z \geq 3$ nm, the vacancy behavior is the same around the twin wall as in the bulk.

The spatial distribution of V_{OX}^- vacancy concentration in the vicinity of the twin-domain-wall/surface junction in CaTiO₃ is shown in Fig. 7. It is seen from the figure that the distribution of V_{OX}^- vacancies is rather complex and strongly affected by the surface.

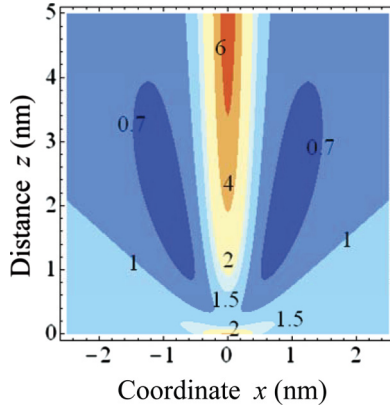


FIG. 7. (Color online) Contour maps of the V_{OX}^- vacancy concentration in the vicinity of the twin-wall/surface junction in CaTiO_3 . The twin-wall plane is $x = 0$. Other parameters are the same as in Fig. 6.

For the used material parameters, the relative contribution of Vegard expansion and flexoelectric coupling into the charged vacancies segregation are of the same order. If the charged vacancies are mobile, they can also contribute to the wall conductivity.

Note that single-charged Ti vacancies concentration near the domain wall can be about 10^3 times higher than the bulk one. This is related with the high values of elastic dipole for these defects.⁸³ Since the equilibrium “bulk” concentration of Ti vacancies should be much smaller than for the oxygen vacancies we showed the figures for the oxygen vacancies only. Neutral vacancies and bi-vacancies cannot change the wall conductivity, but they can be the most thermodynamically stable defects.

VI. SUMMARY

Inhomogeneous elastic strains, which exist due to the rotostriction in the vicinity of the twin-boundary-wall/surface junctions in ferroelastics, can strongly affect their electronic properties. In particular, the strains change the band structure at the wall/surface junction via the deformation potential, rotostriction, and flexoelectric coupling mechanisms. The calculated decrease of the local band gap can be considered as a *direct mechanism* of the uncharged domain-wall conductivity increase in the ferroelastics (CaTiO_3 , EuTiO_3 , SrTiO_3 , etc.), and by extension in other multiferroics (BiFeO_3) and semiconducting ferroelectrics (PbTiO_3 , BaTiO_3 , etc.). Flexoelectric and rotostriction couplings lead to the appearance of

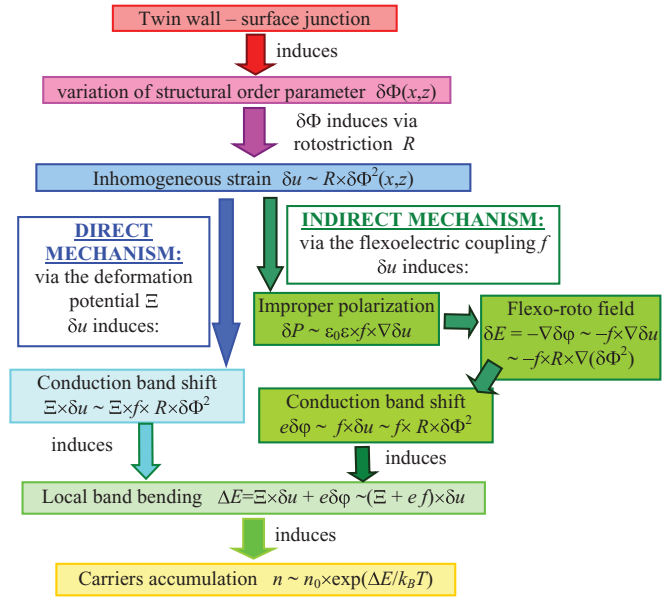


FIG. 8. (Color online) Origin of the twin-domain-wall/ surface junction spontaneous polarization and electroconductivity; direct and indirect mechanisms.

the inhomogeneous electric field, named rotoflexo field,^{35,36} proportional to the structural order parameter gradient across the wall. The fields, which are localized at the domain wall plane and lead to the carrier accumulation in the wall region, are considered as an *indirect mechanism* of the uncharged domain-wall conductivity (see Fig. 8). Comparison of the direct and indirect mechanisms contributions to the twin-wall static conductivity demonstrated their complex interplay in CaTiO_3 . The conductivity response of the twin-wall/surface junction predicted here can be verified by SPM, since the junction is an inherent part of conduction path involved in the probing.

ACKNOWLEDGMENTS

E.A.E. and A.N.M. gratefully acknowledge multiple discussions with N.V. Morozovskii (NAS Ukraine), Nicole Benedek (Cornell University), and Karin Rabe (Rutgers University). V.G. and L.Q.C. acknowledges NSF-DMR-1210588, DMR-0908718, and DMR-0820404 funds. E.A.E. and A.N.M. are thankful to NAS Ukraine and NSF-DMR-0908718 for support. Research supported (S.V.K. and A.B.) by the US Department of Energy, Basic Energy Sciences, Materials Sciences and Engineering Division.

*Corresponding author: morozo@i.com.ua

¹V. M. Fridkin, *Photoferroelectrics* (Springer, 1979).

²J. Kreisel, M. Alexe, and P. A. Thomas, *Nat. Mater.* **11**, 260 (2012).

³R. F. Mamin, *J. Exp. Theor. Phys.* **84**, 808 (1997).

⁴V. M. Fridkin, R. Nitsche, N. Korzhagina, N. A. Kosonogov, R. Magomadov, A. I. Rodin, and K. A. Verkhovskaya, *Phys. Status Solidi A* **54**, 231 (1979).

⁵T. R. Bolk, A. A. Grekov, Kosonogo Na, A. I. Rodin, and V. M. Fridkin, *Soviet Physics Crystallography, Ussr* **16**, 198 (1971).

⁶A. Ohtomo and H. Y. Hwang, *Nature (London)* **427**, 423 (2004).

⁷B. M. Vul, G. M. Guro, and Ivanchik II, *Ferroelectrics* **6**, 29 (1973).

⁸S. Y. Yang, J. Seidel, S. J. Byrnes, P. Shafer, C.-H. Yang, M. D. Rossell, P. Yu, Y.-H. Chu, J. F. Scott, J. W. Ager, L. W. Martin, and R. Ramesh, *Nat. Nanotechnology* **5**, 143 (2010).

- ⁹H. T. Yi, T. Choi, S. G. Choi, Y. S. Oh, and S. W. Cheong, *Adv. Mater.* **23**, 3403 (2011).
- ¹⁰Y. Watanabe, *Ferroelectrics* **419**, 28 (2011).
- ¹¹Y. Watanabe, M. Okano, and A. Masuda, *Phys. Rev. Lett.* **86**, 332 (2001).
- ¹²S. Kaku, H. Eto, K. Nakamura, and Y. Watanabe, ISAF-2009, 18th IEEE *International Symposium on the Applications of Ferroelectrics* (IEEE, New York, 2009), pp. 29–32; Yukio Watanabe, Shigeru Kaku, Daisuke Matsumoto, Yosuke Urakami, and S. W. Cheong, *Ferroelectrics* **379**, 157 (2009).
- ¹³R. F. Mamin, I. K. Bdikin, and A. L. Kholkin, *Appl. Phys. Lett.* **94**, 222901 (2009).
- ¹⁴J. E. Spanier, Alexie M. Kolpak, Jeffrey J. Urban, Ilya Grinberg, Lian Ouyang, Wan Soo Yun, Andrew M. Rappe, and Hongkun Park, *Nano Lett.* **6**, 735 (2006).
- ¹⁵D. B. Li, M. H. Zhao, J. Garra, A. M. Kolpak, A. M. Rappe, D. A. Bonnell, and J. M. Vohs, *Nat. Mater.* **7**, 473 (2008).
- ¹⁶D. D. Fong, A. M. Kolpak, J. A. Eastman, S. K. Streiffer, P. H. Fuoss, G. B. Stephenson, C. Thompson, D. M. Kim, K. J. Choi, C. B. Eom, I. Grinberg, and A. M. Rappe, *Phys. Rev. Lett.* **96**, 127601 (2006).
- ¹⁷G. B. Stephenson and M. J. Highland, *Phys. Rev. B* **84**, 064107 (2011).
- ¹⁸R. V. Wang, D. D. Fong, F. Jiang, M. J. Highland, P. H. Fuoss, C. Thompson, A. M. Kolpak, J. A. Eastman, S. K. Streiffer, A. M. Rappe, and G. B. Stephenson, *Phys. Rev. Lett.* **102**, 047601 (2009).
- ¹⁹J. Shin, V. B. Nascimento, G. Geneste, J. Rundgren, E. W. Plummer, B. Dkhil, S. V. Kalinin, and A. P. Baddorf, *Nano Lett.* **9**, 3720 (2009).
- ²⁰G. I. Guro, I. I. Ivanchik, and N. F. Kovtoniuk, *Sov. Sol. St. Phys.* **11**, 1956 (1969).
- ²¹M. Y. Gureev, A. K. Tagantsev, and N. Setter, *Phys. Rev. B* **83**, 184104 (2011).
- ²²E. A. Eliseev, A. N. Morozovska, G. S. Svechnikov, Venkatraman Gopalan, and V. Ya. Shur, *Phys. Rev. B* **83**, 235313 (2011).
- ²³E. A. Eliseev, A. N. Morozovska, G. S. Svechnikov, Peter Maksymovych, and S. V. Kalinin, *Phys. Rev. B* **85**, 045312 (2012).
- ²⁴M. Mostovoy, K. Nomura, and N. Nagaosa, *Phys. Rev. Lett.* **106**, 047204 (2011).
- ²⁵J. Seidel, L. W. Martin, Q. He, Q. Zhan, Y.-H. Chu, A. Rother, M. E. Hawkrige, P. Maksymovych, P. Yu, M. Gajek, N. Balke, S. V. Kalinin, S. Gemming, F. Wang, G. Catalan, J. F. Scott, N. A. Spaldin, J. Orenstein, and R. Ramesh, *Nat. Mater.* **8**, 229 (2009).
- ²⁶J. Seidel, P. Maksymovych, Y. Batra, A. Katan, S.-Y. Yang, Q. He, A. P. Baddorf, S. V. Kalinin, C.-H. Yang, J.-C. Yang, Y.-H. Chu, E. K. H. Salje, H. Wormeester, M. Salmeron, and R. Ramesh, *Phys. Rev. Lett.* **105**, 197603 (2010).
- ²⁷Nina Balke, Benjamin Winchester, Wei Ren, Ying Hao Chu, Anna N. Morozovska, Eugene A. Eliseev, Mark Huijben, Rama K. Vasudevan, Petro Maksymovych, Jason Britson, Stephen Jesse, Igor Kornev, Ramamoorthy Ramesh, Laurent Bellaiche, Long Qing Chen, and Sergei V. Kalinin, *Nat. Phys.* **8**, 81 (2012).
- ²⁸S. Farokhipoor and B. Noheda, *Phys. Rev. Lett.* **107**, 127601 (2011).
- ²⁹Jill Guyonnet, Iaroslav Gaponenko, Stefano Gariglio, and Patrycja Paruch, *Adv. Mater.* **23**, 5377 (2011).
- ³⁰P. Maksymovych, A. N. Morozovska, P. Yu, E. A. Eliseev, Y. H. Chu, R. Ramesh, A. P. Baddorf, and S. V. Kalinin, *Nano Lett.* **12**, 209 (2012).
- ³¹D. Meier, J. Seidel, A. Cano, K. Delaney, Y. Kumagai, M. Mostovoy, N. A. Spaldin, R. Ramesh, and M. Fiebig, *Nat. Mater.* **11**, 284 (2012).
- ³²V. Ya. Shur, A. V. Ievlev, E. V. Nikolaeva, E. I. Shishkin, and M. M. Neradovskiy, *J. Appl. Phys.* **110**, 052017 (2011).
- ³³P. Maksymovych, J. Seidel, Y. H. Chu, P. P. Wu, A. P. Baddorf, L. Q. Chen, S. V. Kalinin, and R. Ramesh, *Nano Lett.* **11**, 1906 (2011).
- ³⁴Tomas Sluka, Alexander K. Tagantsev, Dragan Damjanovic, Maxim Gureev, and Nava Setter, *Nat. Commun.* **3**, 748 (2012).
- ³⁵A. N. Morozovska, E. A. Eliseev, M. D. Glinchuk, Long-Qing Chen, and Venkatraman Gopalan, *Phys. Rev. B* **85**, 094107 (2012).
- ³⁶A. N. Morozovska, E. A. Eliseev, S. V. Kalinin, Long-Qing Chen, and Venkatraman Gopalan, *Appl. Phys. Lett.* **100**, 142902 (2012).
- ³⁷E. A. Eliseev, A. N. Morozovska, M. D. Glinchuk, B. Y. Zaulychny, V. V. Skorokhod, R. Blinc, *Phys. Rev. B* **82**, 085408 (2010).
- ³⁸E. A. Eliseev, A. N. Morozovska, M. D. Glinchuk, and R. Blinc, *Phys. Rev. B* **79**, 165433, (2009).
- ³⁹A. K. Tagantsev, *Phys. Rev. B* **34**, 5883 (1986).
- ⁴⁰M. S. Majdoub, P. Sharma, and T. Cagin, *Phys. Rev. B* **77**, 125424 (2008).
- ⁴¹Jiawang Hong and David Vanderbilt, *Phys. Rev. B* **84**, 180101(R) (2011).
- ⁴²V. Gopalan and D. B. Litvin, *Nat. Mater.* **10**, 376 (2011).
- ⁴³Jurica Novak and Ekhard K. H. Salje, *J. Phys.: Condens. Matter* **10**, L359 (1998).
- ⁴⁴I. Rychetsky, *J. Phys.: Condens. Matter* **9**, 4583 (1997).
- ⁴⁵Liliana Goncalves-Ferreira, Simon A. T. Redfern, Emilio Artacho, Ekhard Salje, and William T. Lee, *Phys. Rev. B* **81**, 024109 (2010).
- ⁴⁶Craig J. Fennie and Karin M. Rabe, *Phys. Rev. B* **72**, 100103(R) (2005).
- ⁴⁷Nicole A. Benedek and Craig J. Fennie, *Phys. Rev. Lett.* **106**, 107204 (2011).
- ⁴⁸L. Goncalves-Ferreira, Simon A. T. Redfern, Emilio Artacho, and Ekhard K. H. Salje, *Phys. Rev. Lett.* **101**, 097602 (2008).
- ⁴⁹Eric Bousquet, Matthew Dawber, Nicolas Stucki, Celine Lichtensteiger, Patrick Hermet, Stefano Gariglio, Jean-Marc Triscone, and Philippe Ghosez, *Nature (London)* **452**, 732 (2008).
- ⁵⁰Sandra Van Aert, Stuart Turner, Rémi Delville, Dominique Schryvers, Gustaaf Van Tendeloo, and Ekhard K. H. Salje, *Adv. Mater.* **24**, 523 (2012).
- ⁵¹Stephen Jesse, B. J. Rodriguez, Samrat Choudhury, Arthur P. Baddorf, Ionela Vrejoiu, Dietrich Hesse, Marin Alexe, Eugene A. Eliseev, Anna N. Morozovska, Jingxian Zhang, Long-Qing Chen, and Sergei V. Kalinin, *Nat. Mater.* **7**, 209 (2008).
- ⁵²E. A. Eliseev, A. N. Morozovska, S. V. Kalinin, Y. L. Li, Jie Shen, M. D. Glinchuk, L. Q. Chen, and V. Gopalan, *J. Appl. Phys.* **106**, 084102 (2009).
- ⁵³Lun Yang and Kaushik Dayal, *Int. J. Fract.* **174**, 17 (2012).
- ⁵⁴See Supplemental Material at <http://link.aps.org/supplemental/10.1103/PhysRevB.86.085416> for the details of calculations.
- ⁵⁵A. I. Lur'e, *Three-Dimensional Problems of the Theory of Elasticity* (Interscience Publishers, 1964).
- ⁵⁶L. D. Landau and E. M. Lifshitz, *Theory of Elasticity. Theoretical Physics* (Butterworth-Heinemann, Oxford, UK, 1998), Vol. 7.
- ⁵⁷Wenwu Cao and Gerhard R. Barsch, *Phys. Rev. B* **41**, 4334 (1990).
- ⁵⁸N. A. Pertsev, A. K. Tagantsev, and N. Setter, *Phys. Rev. B* **61**, R825 (2000).

- ⁵⁹A. K. Tagantsev, E. Courtens, and L. Arzel, *Phys. Rev. B* **64**, 224107 (2001).
- ⁶⁰Yijia Gu, Karin Rabe, Eric Bousquet, Venkatraman Gopalan, and Long-Qing Chen, *Phys. Rev. B* **85**, 064117 (2012).
- ⁶¹M. A. Carpenter, A. I. Becerro, and Friedrich Seifert, *Am. Mineral.* **86**, 348 (2001).
- ⁶²B. Meyer and David Vanderbilt, *Phys. Rev. B* **65**, 104111 (2002).
- ⁶³G. A. Baker Jr. and P. Graves-Morris, "Pade Approximant" in *Encyclopedia of Mathematics and its Applications*, edited by G.-C. Rota (Addison-Wesley, London, 1981), Vol. 13, 14.
- ⁶⁴P. Zubko, G. Catalan, A. Buckley, P. R. L. Welche, and J. F. Scott, *Phys. Rev. Lett.* **99**, 167601 (2007).
- ⁶⁵W. Ma and L. E. Cross, *Appl. Phys. Lett.* **88**, 232902 (2006).
- ⁶⁶W. Ma and L. E. Cross, *Appl. Phys. Lett.* **79**, 4420 (2001).
- ⁶⁷I. Ponomareva, A. K. Tagantsev, and L. Bellaiche, *Phys. Rev. B* **85**, 104101 (2012).
- ⁶⁸Sh. M. Kogan, *Sov. Phys. Solid State* **5**, 2069 (1964).
- ⁶⁹J. H. Barrett, *Phys. Rev.* **86**, 118 (1952).
- ⁷⁰M. J. Haun, E. Furman, T. R. Halemane, and L. E. Cross, *Ferroelectrics* **99**, 55 (1989), p. 13.
- ⁷¹B. Houchmanzadeh, J. Lajzerowicz, and E. Salje, *J. Phys.: Condens. Matter* **3**, 5163 (1991).
- ⁷²Nicola A. Spaldin and Manfred Fiebig, *Science* **309**, 391 (2005).
- ⁷³C. Herring and E. Vogh, *Phys. Rev.* **101**, 944 (1956).
- ⁷⁴J. Liu, D. D. Cannon, K. Wada, Y. Ishikawa, D. T. Danielson, S. Jongthammanurak, J. Michel, and L. C. Kimerling, *Phys. Rev. B* **70**, 155309 (2004).
- ⁷⁵J. M. Ziman, *Principles of the Theory of Solids* (Cambridge University press, 1972), Chap. 6, item 14.
- ⁷⁶Y. Sun, S. E. Thompson, and T. Nishida, *J. Appl. Phys.* **101**, 104503 (2007).
- ⁷⁷J. S. Lim, X. Yang, T. Nishida, and S. E. Thompson, *Appl. Phys. Lett.* **89**, 073509 (2006).
- ⁷⁸D. D. Nolte, W. Walukiewicz, and E. E. Haller, *Phys. Rev. Lett.* **59**, 501 (1987).
- ⁷⁹N. W. Ashcroft and N. D. Mermin, *Solid State Physics* (Holt, Rinehart and Winston, New York, 1976).
- ⁸⁰Z. Fu, Z. G. Yin, N. F. Chen, X. W. Zhang, H. Zhang, Y. M. Bai, and J. L. Wu, *Phys. Status Solidi RRL* **6**, 37 (2012).
- ⁸¹Robert F. Berger, Craig J. Fennie, and J. B. Neaton, *Phys. Rev. Lett.* **107**, 146804 (2011).
- ⁸²A. N. Morozovska, E. A. Eliseev, A. K. Tagantsev, S. L. Bravina, Long-Qing Chen, and S. V. Kalinin, *Phys. Rev. B* **83**, 195313 (2011).
- ⁸³Daniel A. Freedman, D. Roundy, and T. A. Arias, *Phys. Rev. B* **80**, 064108 (2009).